Testing and Analysis for Lifetime Prediction of Crystalline Silicon PV Modules Undergoing Degradation by System Voltage Stress

Peter Hacke, Ryan Smith, Kent Terwilliger, Stephen Glick, Dirk Jordan, Steve Johnston, Michael Kempe, and Sarah Kurtz

***Abstract*—Acceleration factors are calculated for crystalline silicon photovoltaic modules under system voltage stress by comparing the module power during degradation outdoors with that in accelerated testing at three temperatures and 85% relative humidity. A lognormal analysis is applied to the accelerated lifetime test data, considering failure at 80% of the initial module power. Activation energy of 0.73 eV for the rate of failure is determined for the chamber testing at constant relative humidity, and the probability of module failure at an arbitrary temperature is predicted. To obtain statistical data for multiple modules over the course of degradation *in situ* of the test chamber, dark *I–V* measurements are obtained and transformed using superposition, which is found to be well suited for rapid and quantitative evaluation of potential-induced degradation. It is determined that shunt resistance measurements alone do not represent the extent of power degradation. This is explained with a two-diode model analysis that shows an increasing second diode recombination current and ideality factor as the degradation in module power progresses. Failure modes of the modules stressed outdoors are examined and compared with those stressed in accelerated tests.**

***Index Terms*—Current–voltage (I–V) characteristics, degradation, high-voltage techniques, photovoltaic (PV) cells, photovoltaic systems, reliability.**

I. Introduction

DETERMINATION of the acceleration factors (lifetime at use condition divided by lifetime at accelerated test condition) for the most relevant photovoltaic (PV) module degradation mechanisms is a necessary step for the prediction of module lifetime in the field [1]. The relationship between the time to failure of modules undergoing potential-induced degradation (PID) in the field and those in accelerated tests is not yet clarified. Challenges faced include potentially long periods of time before failure is observed in the field. In addition, obtaining statistical data of module degradation rates in accelerated lifetime testing presents challenges. While some *in situ I–V* testing of modules is being carried out in light-soaking chambers for the study of metastabilities in thin-film modules, analysis for power degradation generally involves intermittently removing the module from chamber and measuring power on a module tester, which is a time-consuming process when numerous samples are involved. In some cases, transients in power performance may occur while a module is waiting for test. It is conceivable that for these reasons, the level of sophistication in degradation rate analyses and service lifetime forecasting in the PV module world has been relatively low. Along with determination of the acceleration factors, comparing fielded and chamber-tested modules with modern analytical and imaging tools will be helpful to choose stress levels for accelerated tests that reproduce failure modes seen in the field.

The high system voltage in series strings of modules was examined as a stress factor that leads to power degradation of crystalline silicon (c-Si) and thin-film amorphous silicon (a-Si) modules by the Jet Propulsion Laboratory beginning in 1978 [2], [3] and again in 2005 by Swanson *et al*. [4] for both rear junction high-efficiency SunPower modules and conventional front junction (n^+/p) c-Si cell modules. The mechanism for degradation of the SunPower module was identified as front surface minority carrier (hole) recombination resulting from a negative charge developing within the cell antireflective layer in positive module arrays [4]. Both c-Si and a-Si modules were shown to degrade as a function of current leaking from the active layer (current generating semiconductor material) of the module through the glass to the grounded module frame [3]. Publications about a-Si outdoor durability, mechanisms, or requirements for testing for system voltage effects include those of BP Solar [5] and Florida Solar Energy Center (FSEC) [6]. a-Si modules have exhibited delamination of the transparent conductive oxide layer because of an accumulation of positively charged Na ions that have migrated toward it from within the soda lime module glass when in negative module arrays [5]. For conventional Si cell modules, SOLON [7] and the National Renewable Energy Laboratory (NREL) [8] characterized the degradation associated with the stress that system voltage bias exerts. Sensitivities to elevated voltage for CdTe modules have also been indicated [9], [10]. NREL [11] and FSEC [12] have reported activation energies for leakage paths associated with degradation by system voltage stress using modules' mounted outdoors. NREL [13] and Fraunhofer ISE [14] have measured these values with environmental chamber tests. Information about the conditions for occurrence and mitigation of system bias degradation on the cell, module,

Manuscript received June 19, 2012; revised August 9, 2012 and September 10, 2012; accepted September 17, 2012. Date of publication November 26, 2012; date of current version December 19, 2012. This work was supported by the U.S. Department of Energy under Contract DE-AC36-08-GO28308 with the National Renewable Energy Laboratory.

The authors are with the National Renewable Energy Laboratory, Golden, CO 80401 USA (e-mail: peter.hacke@nrel.gov; Ryan.Smith@nrel.gov; kent.terwilliger@nrel.gov; Stephen.Glick@nrel.gov; dirk.jordan@nrel.gov; steve.johnston@nrel.gov; Michael.Kempe@nrel.gov; Sarah.Kurtz@nrel.gov).

Color versions of one or more of the figures in this paper are available online at http://ieeexplore.ieee.org.

Digital Object Identifier 10.1109/JPHOTOV.2012.2222351

and system level has also been published [7], [9], [15]. A number of publications suggest the role of positive charges [15], [16], especially Na that is abundant in the module glass [17], [18], as mobile cations accumulating on the near-surface region of the cell leading to failure of the front n^+/p junction of conventional cells by PID in module arrays at negative voltage potential.

In this study, we determine a method to accurately and semi-continuously evaluate the power loss of commercial multicrystalline silicon modules with front junction (n^+/p) cells by PID *in situ* of the dark environmental test chamber, avoiding the need for frequent removal of the modules for *I–V* testing with a solar simulator. Multiple replicas of a module design are stressed in damp heat, varying the temperature level. The degradation rate is modeled so that time to failure can be extrapolated to arbitrary temperatures. Outdoor tests for system voltage durability are performed with the same module design. The degradation rates and degradation modes of the modules tested outdoors are compared with those in accelerated lifetime testing, and acceleration factors are developed. Minimodules are also made and stepped through stresses of increasingly higher temperature and relative humidity (RH) to determine onsets of degradation modes under system voltage bias.

II. Experiment

Environmental chamber testing was carried out on replicas of a conventional mc-Si module at 50 °C, 60 °C, and 85 °C, all at 85% RH. The module nameplate system voltage bias of −600 V was applied continuously to the cells in the module by connecting the shorted leads to a high-voltage (negative) power supply and grounding the module frame [13]. Dark *I–V* curves were obtained with an *I–V* curve tracer capable of resolving five orders of magnitude in current up to 8 A. Curves for each module were obtained periodically *in situ* of the chamber after stabilization of the module temperature to standard test conditions temperature of 25 °C and between 40% and 50% RH and manual disconnection of the high voltage. Ramp rates were 1 °C/m with −600 V applied, and dark $I-V$ measurements were carried out within 1 h of the module reaching 25 °C. Modules were also measured *ex situ* of the chamber for *I–V* testing with a solar simulator to determine the maximum power $P_{\max}$ under 1000-W/m^2 illumination before the start of the stress test, when the fraction power remaining was estimated to be in the range of 0.9–0.95, and again at ∼0.8 or end of test to aid in developing a suitable relationship between the *in situ* electrical characteristics of the module and $P_{\max}$. Modules were generally returned to chamber within 4 h, considering that power recovery of PID has been indicated to be thermally activated based on experiments carried out at 100 °C [7]. The recovery mechanism is not well understood, and some influence of recovery of the modules during the testing for the determination of $P_{\max}$ on our results is conceivable.

Dark *I–V* measurements to evaluate the extent of module degradation in the chamber were recorded *in situ* and analyzed in three ways in Section III-A. Because the degradation mode for PID in p-type base silicon cell modules has been associated with shunting of the cells [7], [8], [15], [19], we first determine if we can calculate the module power during PID from the shunt resistance $R_{\rm sh}$. In the first analytical method, the slope in the vicinity of $V = 0$ is measured to determine *dV/dI* to estimate $R_{\rm sh}$, a simple and convenient gross estimation technique often used by production cell sorters. $R_{\rm sh}$ measurements, using the $I-V$ data around $V_{\rm oc}$, have been used as an indicator for PID in cells [15], but its utility in modules, possibly confounded by bypass diodes and the differences between cells, is not yet clear. The analysis of Fahrenbruch and Bube [20] is applied to estimate the power loss of the module when not too large, whereby the fraction power loss due to $R_{\rm sh}$ is given by $V_{\rm oc}/(J_{\rm sc}\cdot R_{\rm sh})$.

In the second technique, a two-diode model (1) was applied to fit the forward bias dark *I–V* curves of the modules undergoing degradation. $R_{\rm sh}$ and all the other parameters in the model, including pre-exponentials J_{o1} and J_{o2} and ideality factors n_1 and n_2 within the first and second diode terms referred to, respectively, as the diffusion and recombination current densities [21], and the area-specific series resistance R_s, were varied to achieve fitting of the dark *I–V* curve. The ideality factors of the first and second diode terms are often given, respectively in textbooks as 1 and 2. This second diode ideality factor in the recombination current term, 2, controls at medium forward-biases associated with Shockley–Read–Hall recombination at deep traps; however, it has been found that the ideality factor and J_{02} terms further increase in cells with crystallographic defects or a high density of defect states in the p-n junction [21]. Variations in the ideality factor are also linked to lateral (in plane of the device) transport of carriers to defects [22]—these competing effects are not distinguished in this study. The two-diode model dark *I–V* curve fitting has also been described by King and coworkers for analysis of module degradation [23]. As in the first analysis, the evolving $R_{\rm sh}$ is evaluated for the goal of determining the module power degradation

$$J = J_L - J_{01}\left\{\exp\left[\frac{q(V+JR_s)}{n_1 kT}\right]-1\right\} - J_{02}\left\{\exp\left[\frac{q(V+JR_s)}{n_2 kT}\right]-1\right\}+\frac{V+JR_s}{R_{\rm sh}}. \quad (1)$$

The third technique applied was based on superposition—the simplifying assumption that the *I–V* curve obtained in the dark can be translated from the first quadrant to the fourth quadrant by subtracting the photocurrent [24]. Photocurrent (at $J_{\rm sc}$) of the module undergoing PID has been observed to be relatively constant [7], [15]. The maximum power point is then evaluated on the translated *I–V* curve, as conventionally done for curves obtained with solar simulators. This value determined from the dark *I–V* data is compared with the periodically measured power obtained with a solar simulator to determine if a relationship can be made in Section III-B. We then determine how the module power estimated from the dark *I–V* data obtained in the environmental chamber can be used to predictively extrapolate failure times and failure distributions in Section III-C.

Outdoor degradation experiments were performed on replicas of the module design tested in damp heat chambers in Florida, U.S., to obtain representative module performance under the natural stresses of a humid subtropical climate. Variable −600 V

bias was applied to the positive leads of these modules connected to a load resistor, and the voltage was scaled logarithmically with irradiance during the day to simulate the voltage experienced by the cells in the module at highest voltage potential with respect to ground in a negative voltage module string. The modules were mounted horizontally to represent a relatively stressful but realistic flat roof-mounting configuration and the module frames were grounded. The modules were periodically dismounted to evaluate their *I–V* characteristics under a solar simulator. The times to failure of modules stressed outdoors are compared with those of similar modules stressed in the accelerated tests at several temperatures to determine the acceleration factor as a function of temperature in Section III-D.

Finally, in Section III-E, to determine the onset of various failure modes as a function of stress level and to choose stress levels in accelerated testing that are relevant to the degradation modes of fielded modules, a group of one-cell mc-Si minimodules with a conventional construction—glass, ethylene-vinyl acetate, and polyester/polyvinyl fluoride backsheets—were constructed and exposed to increasing levels of temperature and humidity. Details of the power performance of these samples as a function of stress have been previously published [13]. Negative 1000-V bias was first applied to the active layer, followed by a recovery with 1000-V bias, each for 120 h. Testing in both polarities is necessary as cells may show sensitivity to either polarity depending on the cell design [4]. This sequence was repeated incrementally at higher temperature and RH combinations. Carbon-containing paste was applied over the glass face to induce through-glass current flow. This is expected to have the effect of accelerating PID at the lower temperatures and RH, where the glass surface would normally exhibit less conductivity to ground. This arrangement, however, more closely reproduces the high conductivity of a wet glass face and lower internal humidity that a module would experience with rain or dew in the natural environment. The samples were given one week in the chamber at the step level temperature and humidity before voltage was applied. Optical, electroluminescence (EL), and thermal imaging were performed on these samples for failure analysis. In selected cases, photoluminescence imaging was performed to differentiate series resistance and recombination losses.

III. Results and Discussion

A. Estimation of Power Loss From Shunt Resistance

The shunt resistance of a module, as estimated from the value of *dV/dI* in the vicinity of $V = 0$, was measured in the environmental chamber at 25 °C after an exposure to 85% RH, 85 °C, and −600 V bias. The power remaining at the end of the test based on the $R_{\rm sh}$ estimation was $0.942P_{\rm max\_0}$, which correlates very poorly with the actual power drop to $0.765P_{\rm max\_0}$ determined by a solar simulator (see Table I). It is found that the shunt resistance, as captured by the slope in the dark *I–V* curve, does not capture the dominant factor causing the power loss that is observed in the module, and despite the method's attractive simplicity, it does not appear to be a suitable technique to evaluate module power loss from PID.

TABLE I
Shunt Resistance of a Module Degraded by PID Estimated From *dV/dI* at $V \approx 0$ and by the Two-Diode Model, Resulting Fraction Power Loss, and Actual Fraction Power Loss Determined by a Solar Simulator

	d*V*/d*I* at *V*≈0	Two-diode	Solar simulator
$R_{\rm sh}$ (Ω·cm^2)	333	660	
$P_{\rm max}$ /$P_{\rm max\_0}$	0.942	0.971	0.765

The initial shunt resistance of cells within this module was ~6 kΩ·cm^2.

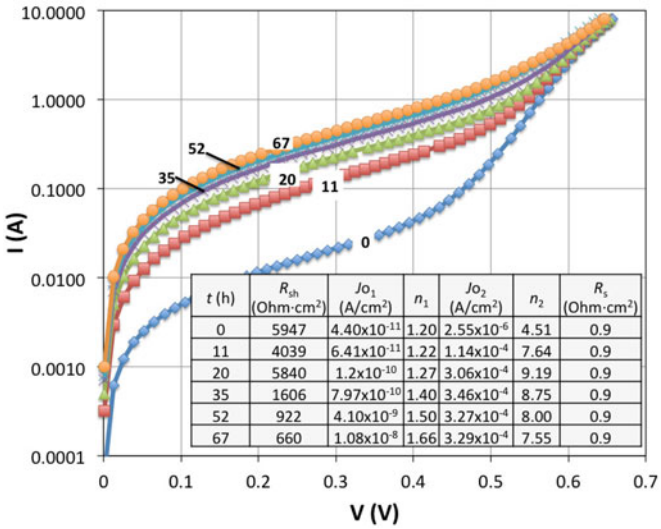

Fig. 1. Evolution of dark I–V curves as a function of time (h), as labeled for a commercial multicrystalline n^+/p silicon cell module stressed in an environmental chamber at 85% RH, 85 °C, and −600 V bias. The curves are measured at 25 °C, and the voltage is indicated on a per-cell basis. Two-diode model fitting parameters, including shunt resistance $R_{\rm sh}$, first and second diode parameters and ideality factors J_0 and n, respectively, and series resistance R_s, are shown in the inset. Translation of the curves significantly upward in the second diode region associated with the progressing degradation dominates; therefore, confidence in the first diode fitting parameters (greater than ~0.45 V) progressively decreases, and R_s obtained at $t = 0$ h is fixed at 0.9 Ω·cm^2.

The entire dark *I–V* curves of modules undergoing PID in chamber were then analyzed by curve fitting to determine the evolution of $R_{\rm sh}$ and other lumped diode parameters of the two-diode model (see Fig. 1). The analysis indicates that the J_{o2} parameter, inclusive of any nonohmic leakage current through the cells, is increasing by two orders of magnitude over the course of the test, ideality factor n_2 increases, and $R_{\rm sh}$ decreases gradually to 660 Ω·cm^2. The module power associated with the $R_{\rm sh}$ decrease calculates out to be only $0.971P_{\rm max\_0}$, compared with $0.765P_{\rm max\_0}$ actual degradation for this module. The increase in the nonlinear recombination current of the second diode term of the two-diode model is thus an important component of PID. For this reason, it appears that using $R_{\rm sh}$ alone will not predict power of the module undergoing PID.

B. Estimation of Power Loss From Superposition of the Dark I–V Curve

The principle of superposition using the dark *I–V* curve was applied for the determination of $P_{\rm max}$. All dark *I–V* curves were translated to the fourth quadrant by 7.3 A (30 mA/cm^2 for the encapsulated 15.6 cm × 15.6 cm area cells). The ratio of the

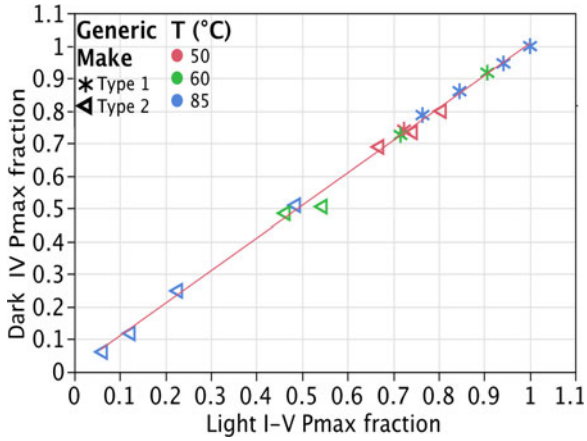

Fig. 2. Correlation between module power $P_{\max}$ determined from the 25 °C dark I–V curves translated to the fourth quadrant (i.e., superposition) and the solar simulator for two module types over the course of PID at −600 V, 85% RH. The correlation is found to be excellent over the whole range of degradation for 13 modules stressed at various temperatures as shown.

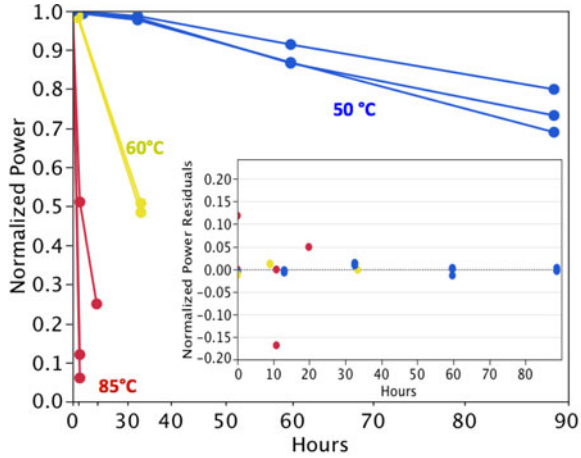

Fig. 3. Normalized power of PV modules undergoing PID at 85% RH, −600 V bias, and at three temperatures indicated on the plot. The data are fit linearly with the time (h) scaled to the power of 2. Residuals to the fit are shown in the inset.

maximum power points obtained after stressing to those of the initial ($t = 0$) translated 25 °C dark I–V curves was compared with the normalized $P_{\max}$ obtained with a solar simulator. These were determined up to three times each for all replicas with two module designs undergoing PID in the environmental chamber, and the correlation was found to be excellent (see Fig. 2). Because we are examining a ratio in the dark I–V analysis, the sensitivity to accuracy of photocurrent inputted into the calculation is mild—a 10% current change results in a 1.6% change in the calculated fraction power remaining in this dataset at around 0.8 $P_{\max\_0}$. Presumably, fine adjustments to the photocurrent value used in the calculations can be made to achieve best fitting of the data if one or more of the actual $P_{\max}$ values during the course of stress testing are obtained with a solar simulator. The dark *I–V* curves can, therefore, be used to estimate the PID *in situ* of the chamber, whereby numerous data points can be obtained, enabling statistical modeling for goals such as service life prediction. This analysis eliminates the need for frequent removal of the module for testing under a solar simulator.

Chamber temperature was ramped to 25 °C for capture of the dark *I–V* curve that was used for the data presented herein. Measurements of *I–V* curves at the elevated stress temperatures were also carried out and translation coefficients to relate $P_{\max}$ obtained at the stress temperature to standard test condition (25 °C) could be used. It is anticipated that such analysis will be developed in more depth in a future publication. Superposition may not be as readily applicable to the *in situ* monitoring of all failure modes in accelerated testing. Despite superposition's success in relating dark *I–V* curves to $P_{\max}$ determined by the solar simulator for the effects of system voltage stress in damp heat in conventional Si modules, further tests are required to determine the applicability of this method to other stress factors, degradation mechanisms, and module types.

C. Degradation Modeling of the Accelerated Lifetime Test Data

The degradation in power of one module design at 85 °C (three replicas), 60 °C (two replicas), and 50 °C (three replicas), 85% RH, and −600 V bias in an environmental chamber was monitored using the estimation of power loss from superposition of the dark *I–V* curves discussed previously. It was found that the power drop could be modeled linearly by transforming the time axis scale to the power of 2, as shown in Fig. 3. The residuals in the linear fitting are shown in the inset. It can be seen that the reproducibility in degradation rates of the various samples is good, with the exception of a few outliers in the most highly accelerated test (85 °C). More work is necessary to derive a mechanistic function, which is anticipated to further improve the degradation curve fitting. Furthermore, automation of the switching between application of the high voltage bias and sweeping of the dark *I–V* curve to increase the frequency of the data taken will better resolve the degradation curves. The degradation data were then analyzed with lognormal statistics, and a lifetime prediction plot was created to calculate the probability of module failure at arbitrary temperatures at 85% RH with a 0.8 $P_{\max\_0}$ failure criterion (see Fig. 4). As an example, the failure probability distribution is calculated and shown for the case of stress at 25 °C, where it is indicated that the peak probability for time to failure is around 550 h. Examining the peaks of the probability distributions, the acceleration in rate to failure of the 85 °C condition over the 60 °C condition is 5.9 times, and the acceleration of the 60 °C condition is 2.3 times that of the 50 °C condition. The density plots, however, show that the data are limited and that more data will be required to improve the certainty in these figures.

D. Degradation Rates of Fielded Modules and Determination of Acceleration Factors

The power as a function of time for two replicas of the module design discussed previously, which was mounted in Florida, U.S., under system voltage bias is shown in Fig. 5. As was done for the accelerated lifetime test data, the power loss is successfully fit linearly with the time scale squared. It is, however, anticipated that differing natural environments in combination with seasonality factors will strongly affect the function of the

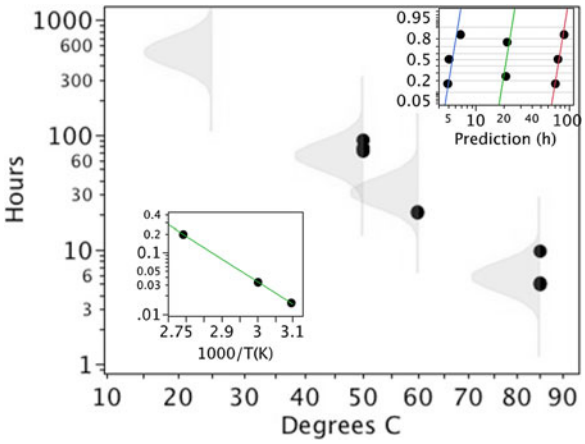

Fig. 4. Lifetime prediction plot as a function of temperature for 85% RH based on failure data interpolated from the degradation curves generated in accelerated lifetime testing. The density curves indicating probability of module failure are shown overlaying the points of failure at the 0.8 $P_{\max\_0}$ level, and the density curve extrapolated to 25 °C is also shown. A multiple probability plot shows a lognormal distribution with the same shape factor to be a good fit to the data (upper right inset). The activation energy for the statistically determined rate of failure is 0.726 ± 0.053 eV (lower left inset).

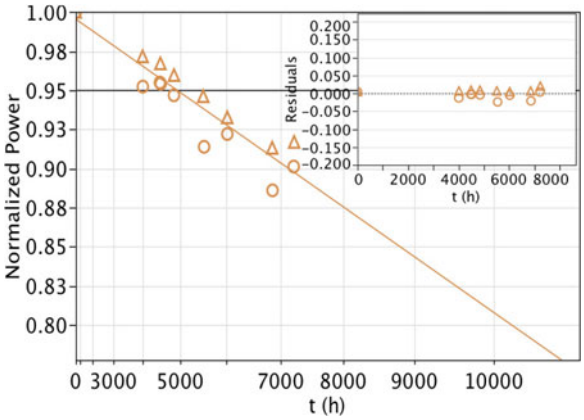

Fig. 5. Fraction power remaining as a function of time under −600-V system voltage bias (applied logarithmically with irradiance) for two module replicas (o, Δ) fielded in Florida for approximately 10 mo, exhibiting PID. For comparison, these modules are of the same design studied in the accelerated lifetime testing.

degradation curve. Failure in this case is taken at $0.95P_{\max\_0}$, which is the degradation limit typical of PV module qualification testing. The alternative, 0.8 $P_{\max\_0}$, a common module warranty limit, leads to censoring, as the modules have only degraded to 0.89 $P_{\max\_0}$ at this writing. The fitting curve in Fig. 5 is nevertheless extrapolated to 0.8 $P_{\max\_0}$, showing the estimation of warranty failure at about 12 000 h (1.37 years).

To determine the time to failure of the fielded module from accelerated lifetime testing, the acceleration factor is calculated—the lifetime at use level divided by lifetime at accelerated stress level. In this case, the use level is the Florida environment, where the degradation as a function of time is shown in Fig. 5 and the accelerated test stress level is 85% RH with temperature levels at 50 °C, 60 °C, and 85 °C, shown in the data of Fig. 3. The system voltage in all cases is −600 V, and the failure is again considered at $0.95P_{\max\_0}$. The calculated acceleration factors determined

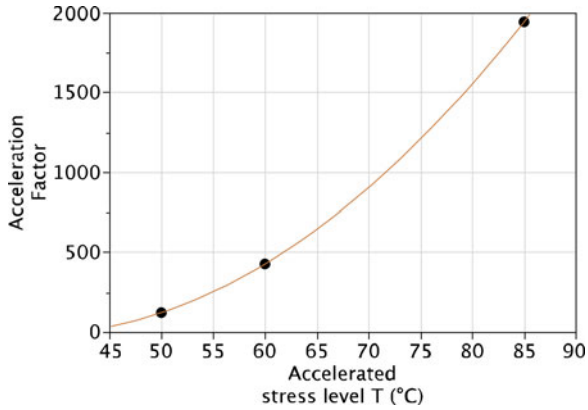

Fig. 6. Acceleration factor for the PV module design mounted in Florida and undergoing accelerated testing at 85% RH, applied module system voltage of −600 V, temperatures as shown, and failure defined at $0.95P_{\max\_0}$. The dominant degradation mode in these modules is PID by junction failure associated with the system voltage bias.

at each stress level of the accelerated tests are graphed in Fig. 6, and the points are interpolated with a fitting curve.

Simplifying assumptions about the relation between the environmental chamber and outdoor tests exist. The indoor tests are done with no illumination; thus, there is no photocurrent. Any possible combined effects, such as that of natural light and the degradation by system voltage stress, are not tested in the darkness of the environmental chamber. The module leads are shorted in the chamber such that the voltage potential between the first and last cells of the series string in the module is the same. Cells within modules mounted outdoors have a modest difference in voltage between the first and last cells of the series string, usually corresponding to the maximum power voltage of the module when regulated by the maximum power tracker of an inverter, or in our experiment, controlled by a load resistor. Constant module nameplate system voltage stress was applied to the modules in chamber at elevated temperature and humidity except for the measurement of dark I–V curves. On the other hand, the modules tested outdoors in this experiment have bias applied that simulates the voltage a series of modules would exert on the module at the last position in an array, up to the module nameplate system voltage under 1-sun irradiance. Module tilt and shading would influence the extent that rainwater flows or dries from the module, affecting degradation rate. These modules experience no bias at night and leakage current from the active layer to ground also falls when the module is dry [13], [14]. They may experience power recovery as a function of increased temperature [7]. Inverter events (grid disturbances, for example) that lead to the array of modules in real systems to be disconnected and placed in an open circuit instead of maximum power voltage may vary and may have influences not captured in this experiment. In this experiment, the module frames are always grounded, but not all PV installations are grounded. For the determination of acceleration factors, a relation is made between environmental chamber tests and outdoor tests with a given module design, natural environment, and simulated voltage stresses that were designed to be as realistic

as possible. The validity of the acceleration factors determined will be controlled by these circumstances.

E. Imaging of Potential-Induced Degradation Modules for Determination of Failure Modes

In the choice of accelerated test conditions, it is necessary to generate the degradation modes that are seen in the field. The commercial modules that were discussed previously exhibit low durability with respect to PID. At the time of their procurement, knowledge about this degradation mode was in its infancy; in fact, at this writing, 70% of modules randomly purchased on the market continue to exhibit strong sensitivity [25]. As modules become more durable to junction failure associated with system voltage stress, stress tests of increasing length are anticipated to evaluate wear out or end of life. Because the commercial modules that were studied previously failed so quickly, mini-modules with cells having higher durability to junction failure under system voltage bias were examined to understand at what stress level failure modes outside of the one we seek to accelerate occur. The degradation modes with voltage bias applied stepping temperature and RH through increasingly higher levels are illustrated in Fig. 7. The time at stress for each level was 120 h (for each polarity), which is relatively short compared with a number of published test-to-failure protocols, such as those calling for 2000 h, 85 °C, 85% RH, with application of the nameplate system voltage [26].

After 50 °C, 50% RH, regions of emerging PID are evident by the new dark regions in the EL and corresponding regions of high current flow through the junction in the thermography (see Fig. 7). After 70 °C, 70% RH, there is evidence of the deep-blue silicon nitride coating giving way to brown or the gray color of silicon at the top of the cell. This is believed to be associated with the decomposition of silicon nitride to hydrous silica and ammonia in the presence of high chemical activity of water [27]. After 85 °C, 85% RH, there is also evidence of series resistance increase in some dark areas of the EL image, considering that the corresponding areas of the thermography indicate cold regions where current does not flow. The series resistance increase is confirmed by photoluminescence imaging of this sample after 85 °C, 85% RH exposure in Fig. 8. The series resistance increase around the upper tab ribbon may be associated with the dissolution of the glass-rich interface between the Ag grid-finger contacts and the silicon cell, enabled by residual acid solder flux placed along the soldered tabs [28], acetic acid from the encapsulant [28], [29], elevated humidity within the package—especially along the cell edge where it is highest, and electrolytic corrosion from the applied voltage bias [17], [30], [31].

Degradation modes of a module stressed outdoors are then examined. Early failures of the most severely stressed modules fielded in Florida under −1500 V bias degraded to 0.35 of the initial power exhibit regions of degraded cell and high current flow through the failed junction by EL and thermography [see Fig. 9(a) and (b)]. Inspecting by photoluminescence confirms the areas of carrier recombination and further shows no regions of high series resistance [see Fig. 9(c) and (d)]. While further study of outdoor failures over many module designs and locations is required, it appears that the 70 °C, 70% RH and greater condition may result in additional failure modes, such as silicon nitride degradation and cell series resistance increases (see Figs. 7 and 8), that are not yet confirmed to occur in the field [see Fig. 9(d)]. Evidence of increased series resistance by dark

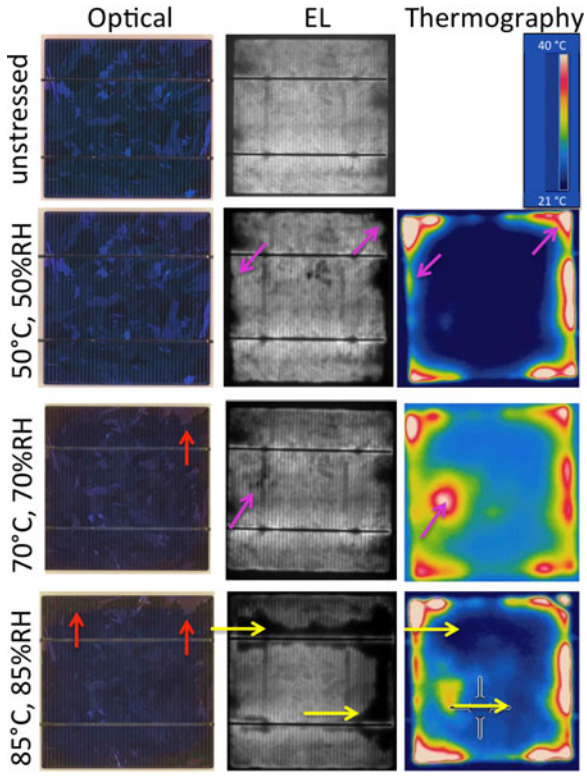

Fig. 7. Imaging—optical, EL under forward bias, and reverse bias thermography—of one-cell minimodules stressed alternately for 120-h periods at ±1000 V, at increasingly higher levels of environmental stress, as shown after the negative bias cycle. After 50 °C, 50% RH exposure, PID by junction leakage is evident by new dark regions in the EL associated with nonradiative recombination and corresponding regions of high current flow through the junction in the thermography indicated by the purple arrows. After 70 °C, 70% RH exposure, there is evidence of silicon nitride degradation at the top face of the cell (red arrow) and additional PID by junction leakage (purple arrows). After 85 °C, 85% RH exposure, there is additional silicon nitride degradation (red arrows) and new evidence of series resistance increase in the dark areas of the EL and the cool areas of the thermography image (yellow arrows).

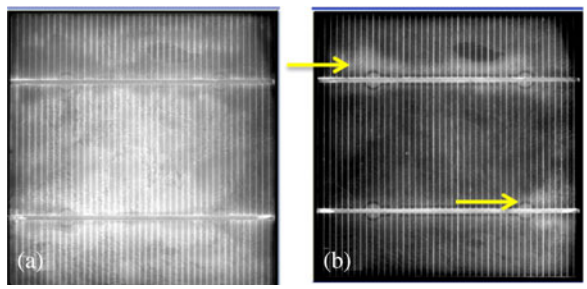

Fig. 8. Photoluminescence of a cell shown in Fig. 7 after exposure at 85 °C, 85% RH, −1000 V bias in environmental chamber stress testing. (a) Cell at open-circuit voltage, where darker regions indicate nonradiative recombination. (b) Short circuit, where light regions, such as those indicated by arrows, indicate elevated series resistance. Both junction recombination or shunting losses and series resistance modes are seen to be active after this stress level.

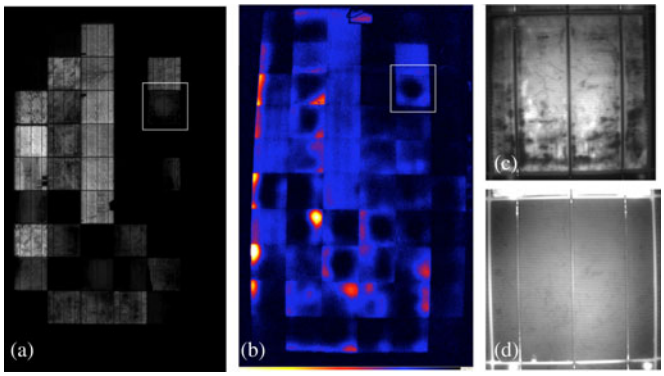

Fig. 9. Module mounted in Florida, after 10 mo with the active layer biased at −1500 V scaled with irradiance, degraded to $0.35P_{\max\_0}$. (a) EL image. (b) Forward bias thermography of the same module (bright areas are hot). (c) Photoluminescence in open circuit of cell indicated by white square (dark areas indicate nonradiative carrier recombination). (d) Photoluminescence in short circuit (light areas indicate elevated series resistance). Gradual gradients across the surface are due to nonuniform illumination; thus, there is no evidence of elevated series resistance in the fielded modules.

I–V curve analysis, EL, and thermal imaging was previously seen in commercial modules after 1000 h 85 °C, 85% RH, with application of 600 or −600 V bias [8] and in an 85 °C, 85% RH environmental chamber, even without the application of system bias [32]. Further exploration of these failure modes in fielded modules is required to find evidence of the modes we seek to accelerate and predict.

IV. Summary and Conclusion

Dark *I–V* curves measured *in situ* in an environmental chamber and analyzed by superposition were used to accurately, rapidly, and statistically evaluate module power during PID. The degradation curves were linearized by evaluating the rate on a time-squared scale and used to model the anticipated lifetime as a function of temperature in 85% RH. The acceleration factor for PID as a function of chamber temperature was determined for a commercial module design at the rated system voltage (−600 V) in Florida so that lifetime associated with the PID failure mode may be forecasted by accelerated testing. It was seen that higher stress levels, such as those around and above 70 °C, 70% RH, led to high chemical activity of water that leads to degradation modes, such as silicon nitride degradation and series resistance increases of the cells, that we have not yet seen in the field.

Acknowledgment

The authors would like to thank A. Anderberg, S. Rummel, K. Emery, F. Yan, B. Sekulic, K. Showalter, and S. Barkaszi for assistance with measurements and helpful discussions and M. Köhl for review of this paper.

References

[1] T. J. McMahon, "Accelerated testing and failure of thin-film PV modules," *Prog. Photovolt: Res. Appl.*, vol. 12, pp. 235–248, 2004.

[2] A. R. Hoffman and R. G. Ross, Jr., "Environmental qualification testing of terrestrial solar cell modules," in *Proc. 13th IEEE Photovoltaic Spec. Conf.*, 1978, pp. 835–842.

[3] G. R. Mon and R. G. Ross, "Electrochemical degradation of amorphous-silicon photovoltaic modules," in *Proc. 18th IEEE Photovoltaic Spec. Conf.*, Las Vegas, NV, 1985, pp. 1142–1149.

[4] R. Swanson, R. Swanson, M. Cudzinovic, D. DeCeuster, V. Desai, Jörn Jürgens , N. Kaminar, W. Mulligan, L. Rodrigues-Barbosa, D. Rose, D. Smith, A. Terao, and K. Wilson, "The surface polarization effect in high-efficiency silicon solar cells," in *Proc. 15th Photovoltaic Solar Energy Conf.*, Shanghai, China, 2005.

[5] J. H. Wohlgemuth, M. Conway, and D. H. Meakin, "Reliability and performance testing of photovoltaic modules," in *Proc. 28th IEEE Photovoltaic Spec. Conf.*, 2000, pp. 1483–1486.

[6] N. G. Dhere. (2011). High voltage bias testing of specially designed c-Si PV modules, in *Proc. Photovoltaic Module Reliabil. Workshop*. [Online]. Available: www.eere.energy.gov/solar/pv_module_reliability_workshop_2011.html

[7] S. Pingel, O. Frank, M. Winkler, S. Daryan, T. Geipel, H. Hoehne, and J. Berghold, "Potential induced degradation of solar cells and panels," in *Proc. 35th IEEE Photovoltaic Spec. Conf.*, Honolulu, HI, Jun. 2010, pp. 2817–2822.

[8] P. Hacke, K. Terwilliger, S. Glick, D. Trudell, N. Bosco, S. Johnston, and S. Kurtz, "Test-to-failure of crystalline silicon modules," in *Proc. 35th IEEE Photovoltaic Spec. Conf.*, Honolulu, HI, Jun. 2010, pp. 244–250.

[9] C. R. Osterwald, T. J. McMahon, and J. A. del Cueto, "Electrochemical corrosion of SnO_2:F transparent conducting layers in thin-film photovoltaic modules," *Sol. Energy Mater. Sol. Cells*, vol. 79, pp. 21–33, 2003.

[10] M. Beck, P. Gonzalez, R. Gruber, and J. Tyler, (2011). "Thin film module reliability-enabling solar electric generation," in *Proc. Photovoltaic Module Reliab. Workshop*. [Online]. Available: www1.eere.energy.gov/solar/pdfs/pvmrw2011_03_plen_beck.pdf

[11] J. A. DelCueto and T. J. McMahon, "Analysis of leakage currents in photovoltaic modules under high-voltage bias in the field," *Prog. Photovolt: Res. Appl.*, vol. 10, pp. 15–25, 2002.

[12] N. G. Dhere, S. M. Bet, and H. P. Patil, "High-voltage bias testing of thin-film PV modules," in *Proc. 3rd World Conf. Photovoltaic Energy Convers.*, 2003, pp. 1923–1926.

[13] P. Hacke, K. Terwilliger, R. Smith, S. Glick, J. Pankow, M. Kempe, and S. Kurtz, "System voltage potential-induced degradation mechanisms in PV modules and methods for test," in *Proc. 37th IEEE Photovoltaic Spec. Conf.*, Seattle, WA, Jun. 2011, pp. 814–820.

[14] S. Hoffmann and M. Koehl, "Effect of humidity and temperature on the potential-induced degradation," *Prog. Photovolt: Res. Appl.*, 2012, doi: 10.1002/pip.2238.

[15] H. Nagel, A. Metz, and K. Wangemann, "Crystalline Si solar cells and modules featuring excellent stability against potential-induced degradation," presented at the 26th Eur. Photovoltaic Solar Energy Conf. Exhib., Hamburg, Germany, 2011.

[16] M. Schütze, M. Junghänel, O. Friedrichs, R. Wichtendahl, M. Scherff, J. Müller, and P. Wawer, "Investigations of potential induced degradation of silicon photovoltaic modules," presented at the 26th Eur. Photovoltaic Solar Energy Conf., Hamburg, Germany, Sep. 5–9, 2011.

[17] P. Hacke, M. Kempe, K. Terwilliger, S. Glick, N. Call, S. Johnston, and S. Kurtz, "Characterization of multicrystalline silicon modules with system bias voltage applied in damp heat," in *Proc. 25th Eur. Photovoltaic Solar Energy Conf. Exhib./5th World Conf. Photovoltaic Energy Convers.*, Valencia, Spain, Sep. 6–10, 2010, pp. 3760–3765.

[18] J. Bauer, V. Nauman, S. Großer, C. Hagendorf, M. Schütze, and O. Breitenstein, "On the mechanism of potential-induced degradation in crystalline silicon solar cells," *Phys. Status Solidi: Rapid Res. Lett.*, vol. 6, pp. 331–333, 2012.

[19] M. Schütze, M. Junghänel, M. B. Koentopp, S. Cwikla, S. Friedrich, J. W. Müller, and P. Wawer, "Laboratory study of potential induced degradation of silicon photovoltaic modules," in *Proc. 37th IEEE Photovoltaic Spec. Conf.*, Seattle, WA, 2011, pp. 000821–000826.

[20] A. L. Fahrenbruch and R. H. Bube, *Fundamentals of Solar Cells: Photovoltaic Solar Energy Conversion*. New York: Academic, 1983, pp. 220–222.

[21] O. Breitenstein, J. Bauer, P. P. Altermatt, and K. Ramspeck, "Influence of defects on solar cell characteristics," *Solid State Phenomena*, vol. 156–158, pp. 1–10, 2010.

[22] K. R. MacIntosh, "Lumps, humps and bumps: Three detrimental effects in the current-voltage curve of silicon solar cells," Ph.D. dissertation, UNSW, Cent. Photovoltaic Eng., Sch. Electr. Eng., 2011.

[23] D. L. King, B. R. Hansen, J. A. Kratochvil, and M. A. Quintana, "Dark current–voltage measurements on photovoltaic modules as a diagnostic or manufacturing tool," in *Proc. 26th IEEE Photovoltaic Spec. Conf.*, Sep.–Oct. 1997, pp. 1125–1128.

[24] M. Wolf and H. Rauschenbach, "Series resistance effects on solar cell measurements," in *Advanced. Energy Conversion*. vol. 3, London, U.K.: Pergamon, 2013, pp. 455–479.

[25] J. Bagdahn, M. Ebert, J. Fröbel, and S. Dietrich, "Test results of potential induced degradation (PID) of solar modules from different manufacturers," Fraunhofer Center Silicon Photovolt, Freiburg, Germany Tech. Rep., Jun. 2012, Available: http://www.en.csp.fraunhofer.de/presse-und-veranstaltungen/details/id/51/

[26] A. Funcell. (Feb. 28–Mar. 1, 2012). The thresher test crystalline silicon terrestrial photovoltaic (PV) modules long term reliability and degradation, in *Proc. NREL Photovoltaic Module Reliab. Workshop* Golden, CO [Online]. Available: http://www.nrel.gov/ce/ipvmqa_forum/pdfs/14-ipvmqaf_funcell_renewable_energy_test_center.pdf

[27] K. Morita and K. Ohnaka, "Novel selective etching method for silicon nitride films on silicon substrates by means of subcritical water," *Ind. Eng. Chem. Res.*, vol. 39, pp. 4684–4688, 2000.

[28] K. Whitfield, A. Salomon, S. Yang, and I. Suez, "Damp heat versus field reliability for crystalline silicon," presented at the 38th IEEE Photovoltaic Spec. Conf., Austin, TX, 2012.

[29] A. W. Czanderna and F. J. Pern, "Encapsulation of PV modules using ethylene vinyl acetate copolymer as a pottant: A critical review," *Sol. Energy Mater. Sol. Cells*, vol. 43, pp. 101–181, 1996.

[30] G. R. Mon. (1983). Observations of solar-cell metallization corrosion, in *Proc. Flat-Plate Solar Array Res. Forum Photovoltaic Metallization Syst.* [Online]. pp. 137–146. Available: http://ntrs.nasa.gov

[31] G. R. Mon, L. Wen, R. G. Ross, Jr., and D. Adent, "Effects of temperature and moisture on module leakage current," in *Proc. 18th IEEE Photovoltaic Spec. Conf.*, 1985, pp. 1179–1185.

[32] K. Whitfield and A. Salomon. (2011). "Modeling based on Damp Heat Testing," in *Proc. Photovoltaic Module Reliab. Workshop*, pp. 1–25. [Online]. Available: http://www1.eere.energy.gov/solar/pdfs/pvmrw12_tuespm_solaria_whitfield.pdf, accessed Sep. 9, 2012

Authors' photographs and biographies not available at the time of publication.